Optics Letters

Observation on temperature and strain dependency of Brillouin dynamic grating in a few-mode fiber with a ring-cavity configuration

Yinping Liu,[1,2] Guangyao Yang,[1,2] Ning Wang,[2] Lin Ma,[1,*] J. C. Alvarado-Zacarias,[2] J. E. Antonio-Lopez,[2] Pierre Sillard,[3] A. Amezcua-Correa,[3] R. Amezcua-Correa,[2] Xinyu Fan,[1] Zuyuan He,[1] and Guifang Li[2]

[1]State Key Laboratory of Advanced Optical Communication Systems and Networks, Shanghai Jiao Tong University, Shanghai 200240, China
[2]CREOL, The College of Optics and Photonics, University of Central Florida, Orlando, Florida 32816, USA
[3]Prysmian Group, Parc des Industried Artois Flandres, Douvrin 62138, France
*Corresponding author: ma.lin@sjtu.edu.cn

Received 20 January 2020; accepted 2 March 2020; posted 4 March 2020 (Doc. ID 388739); published 6 April 2020

We experimentally conduct Brillouin dynamic grating (BDG) operation using a 1-km-long four-mode fiber. By employing a simplified ring-cavity configuration with single-end pumping, the BDG is effectively generated in LP_{01} mode within a range of 250 m, and three higher-order modes, namely, LP_{11b}, LP_{21a}, and LP_{02}, are chosen as probes to analyze the BDG with a spatial resolution of 1 m. To the best of our knowledge, this is the first time to characterize the responses of BDG frequency to temperature and strain for different modes in a conventional few-mode fiber. By employing the pump–probe pair of LP_{01}−LP_{02} mode, the highest temperature and strain sensitivities of 3.21 MHz/°C and −0.0384 MHz/με have been achieved. Also, the performance of simultaneously distributed temperature and strain sensing based on BDG is evaluated.

https://doi.org/10.1364/OL.388739

Stimulated Brillouin scattering (SBS) is capable of generating a traveling tunable Bragg grating, called Brillouin dynamic grating (BDG), by periodically modulating the refractive index of fiber [1]. The BDG has been intensely investigated for its potential in various applications, such as optical tunable delay line, all-optical signal processing, and optical storage [2,3]. It is also regarded as an effective method for distributed fiber-optic sensing. By generating BDG in a polarization-maintaining fiber (PMF) with pumps of one polarization state and analyzing BDG with an orthogonally polarized probe light, the spatial resolution of Brillouin optical time domain analysis (BOTDA) can be dramatically improved to 1 cm [4]. Also, since the BDG frequency and Brillouin frequency shift (BFS) react to strain in the same direction while having opposite dependences on temperature, they are simultaneously measured to achieve a complete discrimination between temperature and strain [5]. However, the PMF-BDG scheme, which requires an all-polarization-maintaining configuration, will inevitably increase the overall cost. By controlling the polarization of pump and probe, the BDG operation is conducted over a standard single-mode fiber (SMF) [6]. Due to the intrinsic random birefringence of SMF, the BDG in SMF is hard to employ for distributed sensing. Few-mode fibers (FMFs) have also been considered as promising sensing media because they can support more than one orthogonal spatial mode [7]. The BDG operation in a polarization-maintaining elliptical-core two-mode fiber has been demonstrated [8,9]. By using the two orthogonal polarizations of the LP_{01} mode as pumps, respectively, and detecting the BDG with one polarization of the LP_{11} mode, a simultaneous temperature and strain sensing is achieved with an accuracy of 1.6°C and 105 με. On the other hand, the BDG responses to temperature and strain for different spatial modes in a conventional FMF have not been explored yet.

In this Letter, we perform the BDG operation in a four-LP-mode fiber. A simplified ring-cavity configuration with a single-end pump is employed to build up BDG efficiently. The BDG is generated through the LP_{01} mode and analyzed by three higher-order modes. Also, the temperature and strain coefficients of BDG frequency shift for different modes are characterized. The highest temperature and strain sensitivities of 3.21 MHz/°C and −0.0384 MHz/με are realized by using LP_{02} mode as the probe. Distributed temperature and strain measurements based on BDG are experimentally demonstrated with a 1-m spatial resolution in a range of 250 m. To the best of our knowledge, this is the first observation on the temperature and strain coefficients of BDG frequency in a four-mode fiber with different higher-order modes as the probe. Also, the performance of discriminative temperature and strain sensing has also been investigated.

Figure 1 shows the operation principle of the proposed scheme. The BDG is generated by the SBS in mode i based on a ring cavity and analyzed by the higher-order mode j. When the pump at the frequency of ν_i goes through the FMF in the anti-clockwise direction, the Stokes wave that experiences a

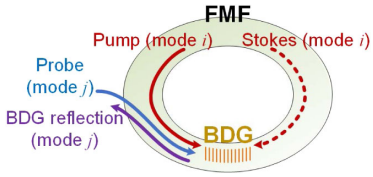

Fig. 1. Principle of BDG operation in an FMF ring cavity.

frequency downshift of $\Delta\nu_B$ will travel in the clockwise direction and act as the counter-propagating pump contributing to stimulate the acoustic wave. Here, $\Delta\nu_B$ is equal to the BFS of the FMF, which can be expressed as

$$\Delta\nu_B = 2n_i\nu_i V_a/c, \tag{1}$$

where n_i is the effective refractive index (ERI) of mode i, V_a is the acoustic velocity in the fiber core, and c is the speed of light. By employing a ring cavity configuration, the circulating Stokes wave can accumulate enough gain from the pump, and the intramodal Brillouin lasing can be realized when the pump power reaches the threshold [10]. As a result, the BDG can be effectively built up. If a probe propagating in the same direction as the pump is launched into the FMF in mode j, it can be reflected by the BDG when the pump–probe frequency deviation satisfies the phase-match condition:

$$\nu_D = \nu_j - \nu_i = \Delta n_{ij}\cdot\nu_i/n_i, \tag{2}$$

where ν_D is the frequency deviation between the pump and probe called BDG frequency, and Δn_{ij} is regarded as the intermodal birefringence. When the BDG is analyzed by mode j, the relationship between the variation of BDG frequency ($\Delta\nu_D$) and the change of temperature and axial strain (ΔT, ΔE) can be approximately expressed as

$$\Delta\nu_D = C_T^{i,j}\cdot\Delta T + C_E^{i,j}\cdot\Delta E, \tag{3}$$

where C_T and C_E are the temperature and strain coefficients, respectively. As a result, the temperature and strain profile along the fiber can be obtained through the variation of BDG frequency. Furthermore, the simultaneous temperature and strain sensing could be realized in the case that there exists a significant discrepancy in the temperature and strain coefficients among different mode combinations.

The experimental setup is shown in Fig. 2. A tunable laser source (TLS) (Santec TSL-210) was used as the light for the pump, and the output light was amplified by an erbium-doped fiber amplifier (EDFA). The polarization state of the pump and Stokes wave was aligned using polarization controllers (PCs) in order to maximize the SBS intensity. The fiber under test (FUT) is a 1-km-long step-index (SI) four-LP-mode FMF with a core diameter of 15 μm, which can support six degenerate modes (LP_{01}, LP_{11a}, LP_{11b}, LP_{21a}, LP_{21b}, and LP_{02}). The FUT consists of a 250-m-long sensing fiber and a 750-m-long dummy fiber, which is temperature controlled to generate the Stokes wave stably. The fundamental mode of the input fiber can evolve into the desired mode of the FMF by using the mode-selective photonic lantern (MSPL) as described in [11]. The measured insertion losses of the MSPL1 at a wavelength of 1550 nm are 1.71, 3.75, 1.79, 2.29, 1.46, and 4.35 dB for LP_{01}, LP_{11a}, LP_{11b}, LP_{21a}, LP_{21b}, and LP_{02} modes, respectively, resulting mainly from the imperfect tapering process and the mode field

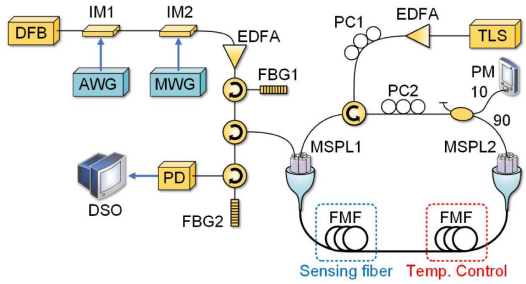

Fig. 2. Experimental setup. DFB, distributed feedback laser; EDFA, erbium-doped fiber amplifier; IM, intensity modulator; AWG, arbitrary waveform generator; MWG, microwave generator; FBG, fiber Bragg grating; TLS, tunable laser source; PM, power meter; MSPL, mode-selective photonic lantern; PD, photo-detector; PC, polarization controller; and DSO, digital oscilloscope.

mismatch. Figure 3(a) depicts the refractive index profile of the FUT, and Figs. 3(b)–3(g) show the observed near-field mode patterns for different modes at 1550 nm. The pump was launched into the LP_{01} port of MSPL1 through a circulator, and the backscattering Stokes wave was amplified by the intramodal SBS effect in the ring cavity. Figure 4(a) shows the power of the Stokes wave as a function of the pump power in LP_{01} mode. It can be observed that the conversion efficiency is about 60%. In our experiment, the pump power was set to be 510 mW, corresponding to a Stokes power of around 290 mW. Also, the frequency difference between the Stokes wave and pump is determined by the BFS of the dummy fiber, since the sensing fiber is too short to generate a stable Stokes wave. We measured the relationship between the frequency difference and temperature of the dummy fiber, as shown in Fig. 4(b). The result indicates the possibility to adjust $\Delta\nu_B$ to generate BDG in the sensing fiber with arbitrary BFS. To analyze the generated BDG, a distributed-feedback (DFB) laser was used as the light source. The probe wave was first modulated into pulses using an intensity modulator (IM) driven by an arbitrary waveform generator (AWG). The pulse repetition rate was set to be 250 kHz, and the pulse width was 10 ns, which corresponds to a spatial resolution of 1 m. Another IM and a microwave generator (MWG) were employed to generate a double-side-band (DSB) signal, where one sideband was removed by a fiber Bragg grating (FBG), which had a bandwidth of 0.16 nm, and the other sideband was amplified by an EDFA. The probe pulse with a peak power of 3.5 W was launched into the MSPL1 through a circulator and evolved into a particular mode to analyze the BDG. Among the five higher-order spatial modes, LP_{11b}, LP_{21a}, and LP_{02} modes were selected to be probes due to their relatively low insertion loss, which contributes to a high SNR in BDG measurement. To locate the reflection frequency of the BDG for different probe modes, we tuned the center wavelength of TLS and monitored

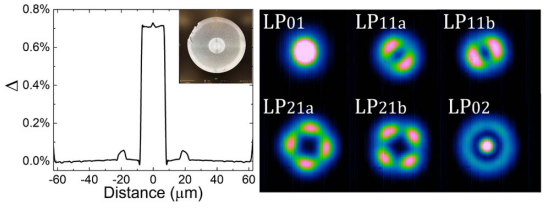

Fig. 3. Measured refractive index profile of the FUT and the near-field mode patterns of six supported modes.

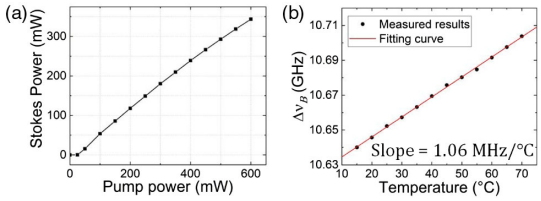

Fig. 4. (a) Dependence of Stokes power on pump power and (b) $\Delta\nu_B$ as a function of the temperature of the dummy fiber.

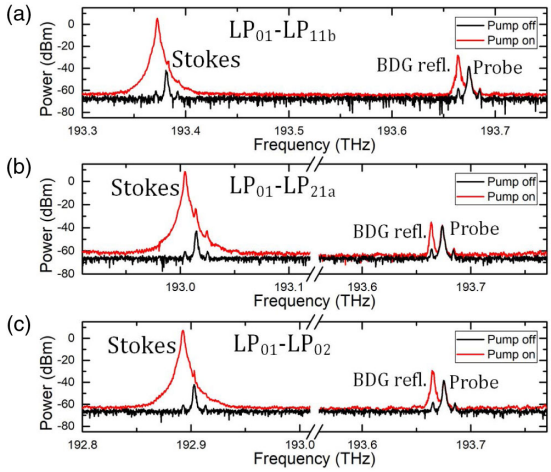

Fig. 5. Optical spectra of BDG reflection by probing through (a) LP_{11b} mode, (b) LP_{21a} mode, and (c) LP_{02} mode.

the reflected optical spectrum before the FBG filter. As shown in Fig. 5, when the frequency deviations between the pump in LP_{01} mode and probes in LP_{11b}, LP_{21a}, and LP_{02} modes were tuned to be around 293.6, 667.2, and 773.7 GHz, which correspond to an intermodal birefringence of 2.19e-3, 4.98e-3, and 5.77e-3, respectively, the phase-matching conditions were approximately satisfied, and the reflected signals at the frequency that downshifted 10.65 GHz from the probes could be obviously observed. The frequency downshift results from the Doppler effect of BDG moving, which is the same for all probe modes. By continuously sweeping the output frequency of the MWG within a range of 4 GHz during a period of 8 ms, the reflected spectra were characterized with a 2-MHz resolution. We used another FBG to filter the unwelcome signals in front of the photo-detector (PD) (Thorlabs PDA05CF2), which had a bandwidth of 150 MHz. The output signal of PD was then recorded by a digital sampling oscilloscope (DSO) with a sampling rate of 250 MS/s. The recorded traces were averaged by 1000 times.

Figures 6(a)–6(c) show the BDG spectra distributions along the FUT for different pump–probe combinations. Due to the nonuniformity along the FUT introduced by the fabrication and winding process, the dominant reflection peak changes randomly within a range of 4 GHz at different positions, corresponding to an ERI variation of 3e-5. The BDG spectra for the combinations of $LP_{01}-LP_{21a}$ and $LP_{01}-LP_{02}$ show a wider spread, mainly because the ERIs of LP_{21a} mode and LP_{02} mode are more sensitive to the fiber deformation. Figures 7(a)–7(c) depict the BDG reflection spectra for different pump–probe pairs at the distance of 200 m. The BDG spectra can be observed

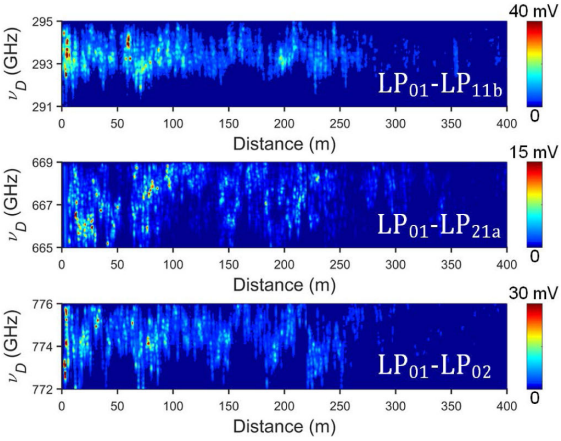

Fig. 6. BDG spectrum distributions along the FUT for different pump–probe mode combinations.

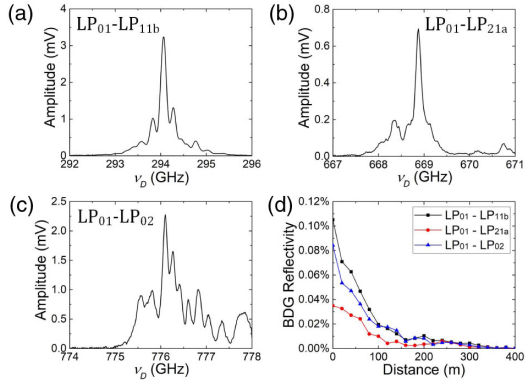

Fig. 7. BDG reflection spectra at the distance of 200 m for pump–probe pairs of (a) $LP_{01}-LP_{11b}$, (b) $LP_{01}-LP_{21a}$, and (c) $LP_{01}-LP_{02}$ mode, and (d) BDG reflectance versus fiber length.

in a range of 3 GHz with multiple reflection peaks, which can be attributed to the nonuniform intermodal birefringence along the FUT as well as the birefringence between degenerate modes. Figure 7(d) depicts the calculated reflectance versus distance for different pump–probe pairs. Owing to the depletion of pump power, the BDG exists mainly in the first 300 m of the FUT, and the reflectance decreases rapidly along with the FUT. Also, the BDG reflectance with the probe of LP_{11b} or LP_{02} mode is much higher than that with the LP_{21a} mode probe, which is influenced by the overlap integral between the optical and acoustic fields.

In order to demonstrate the distributed sensing with the proposed technique, a segment of 2-m-long FUT at the distance of 200 m was placed into a temperature controllable water bath. Another segment of 2-m-long FUT was fixed to a pair of displacement stages for exerting strain at the distance of 205 m. Figure 8 illustrates the distributions of BDG frequency shift $\Delta\nu_D$ along the fiber with and without applying temperature or strain. A high visibility is achieved with the pump–probe pairs of $LP_{01}-LP_{11b}$ and $LP_{01}-LP_{02}$ mode, which show the potential for temperature and strain discrimination since they exhibit different responses to temperature and strain. The cross-correlation of BDG spectra was calculated to estimate $\Delta\nu_D$ due to the irregular BDG spectrum with multiple-peak structure. The standard deviations of $\Delta\nu_D$ at the end of the sensing fiber

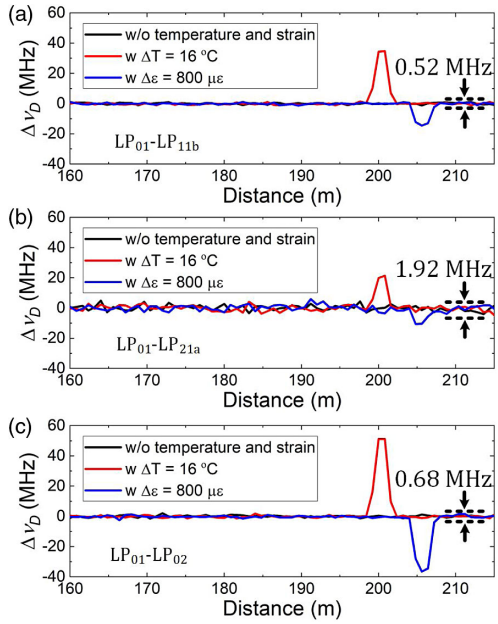

Fig. 8. Distribution of BDG frequency shift along the fiber under different temperatures and strains.

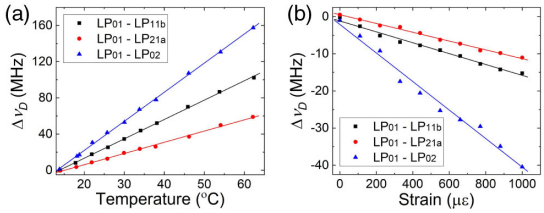

Fig. 9. Measured $\Delta\nu_D$ as a function of (a) temperature and (b) strain.

are 0.52, 1.92, and 0.68 MHz for the pump–probe pairs of $LP_{01}-LP_{11b}$, $LP_{01}-LP_{21a}$, and $LP_{01}-LP_{02}$, respectively.

Figure 9 shows the calculated frequency shift $\Delta\nu_D$ as a function of (a) temperature and (b) strain with different pump–probe pairs. The calculated temperature and strain coefficients are shown in Table 1. The combination of LP_{01} and LP_{02} modes exhibits the highest temperature and strain sensitivities of 3.21 MHz/°C and −0.0384 MHz/με as well as the best accuracy of 0.22°C and 18 με. The discrepancy of coefficients among different pump–probe combinations allows the simultaneous temperature and strain measurement, but the accuracy may be deteriorated in the decoupling process [12]. By employing the combinations of $LP_{01}-LP_{11b}$ and $LP_{01}-LP_{02}$, respectively, the temperature and strain can be separately obtained with an accuracy of 0.61°C and 60.7 με. The accuracy deterioration factor of several typical schemes, which is defined as the ratio of the measurement accuracy with and without a decoupling process, is calculated and shown in Table 2. Due to the insufficient discrepancy of coefficients, the accuracy may be deteriorated by around three times when it comes to realizing the discriminated measurement in our experiment. An improved accuracy can be expected by combining the BDG and BOTDA in FMF.

Table 1. Temperature and Strain Coefficients

Probe Mode	Temperature (MHz/°C)	Strain (MHz/με)
LP_{11b}	2.14	−0.0143
LP_{21a}	1.17	−0.0121
LP_{02}	3.21	−0.0384

Table 2. Accuracy Deterioration Factors of Different Schemes

	Accuracy Deterioration Factor	
Scheme	Temperature	Strain
FMF-BDG	2.77	3.37
PMF-BDG [5]	0.80	0.88
FMF-BOTDA [13]	8.51	9.18

In conclusion, we have experimentally investigated BDG operation in a conventional four-mode FMF and demonstrated the distributed temperature and strain sensing based on BDG with 1-m spatial resolution in a range of 250 m. By employing the ring-cavity configuration with single-end pumping, the BDG is effectively generated by SBS in LP_{01} mode, while three higher-order modes are used as probes to analyze the BDG. The temperature and strain coefficients for different modes are obtained for the first time. With the pump–probe pair of $LP_{01}-LP_{02}$ mode, the temperature and strain sensitivities of 3.21 MHz/°C and −0.0384 MHz/με are achieved, respectively. Also, the feasibility of simultaneous temperature and strain sensing with BDG in FMF has been investigated.

Funding. National Natural Science Foundation of China (61775132, 61775138, 61975116); China Scholarship Council.

Disclosures. The authors declare no conflicts of interest.

REFERENCES

1. K. Y. Song, W. Zou, Z. He, and K. Hotate, Opt. Lett. **33**, 926 (2008).
2. K. Y. Song, K. Lee, and S. B. Lee, Opt. Express **17**, 10344 (2009).
3. Z. Zhu, D. J. Gauthier, and R. W. Boyd, Science **318**, 1748 (2007).
4. K. Y. Song, S. Chin, N. Primerov, and L. Thevenaz, J. Lightwave Technol. **28**, 2062 (2010).
5. W. Zou, Z. He, and K. Hotate, Opt. Express **17**, 1248 (2009).
6. K. Y. Song, Opt. Lett. **36**, 4686 (2011).
7. S. Li, M.-J. Li, and R. S. Vodhanel, Opt. Lett. **37**, 4660 (2012).
8. Y. H. Kim and K. Y. Song, Opt. Lett. **42**, 3036 (2017).
9. Y. H. Kim and K. Y. Song, Opt. Express **22**, 17292 (2017).
10. N. Wang, J. C. Alvarado-Zacarias, M. S. Habib, H. Wen, Y. Zhang, J. E. Antonio-Lopez, P. Sillard, A. Amezcua-Correa, R. Amezcua-Correa, and G. Li, in *Conference on Lasers and Electro-Optics* (Optical Society of America, 2019), paper SM1L.1.
11. A. M. Velazquez-Benitez, J. C. Alvarado, G. Lopez-Galmiche, J. E. Antonio-Lopez, J. Hernández-Cordero, J. Sanchez, P. Sillard, C. M. Okonkwo, and R. Amezcua-Correa, Opt. Lett. **40**, 1663 (2015).
12. W. Jin, W. C. Michie, G. Thursby, M. Konstantaki, and B. Culshaw, Opt. Eng. **36**, 598 (1997).
13. A. Li, Y. Wang, J. Fang, M.-J. Li, B. Y. Kim, and W. Shieh, Opt. Lett. **40**, 1488 (2015).